Food and Chemical Toxicology 210 (2026) 115981

Contents lists available at ScienceDirect

Food and Chemical Toxicology

journal homepage: www.elsevier.com/locate/foodchemtox

# Gastrointestinal permeability and hepatic mechanisms of toxicity of chloro-cathinones

Mariana Meneses [a,b,c], Inês Ferreira [b,c,d], Ana Patrícia Gomes [b,c,d], Rita Pacheco [b,d,*,1], Helena Gaspar [a,c,**,1]

[a] Departamento de Química e Bioquímica, Faculdade de Ciências, Universidade de Lisboa, 1749-016, Lisboa, Portugal
[b] Centro de Química Estrutural, Institute of Molecular Sciences, Faculdade de Ciências, Universidade de Lisboa, 1749-016, Lisboa, Portugal
[c] BioISI – Biosystems and Integrative Sciences Institute, Faculdade de Ciências, Universidade de Lisboa, 1749-016, Lisboa, Portugal
[d] Departamento de Engenharia Química, Instituto Superior de Engenharia de Lisboa, Av. Conselheiro Emídio Navarro, 1959-007, Lisboa, Portugal

ARTICLE INFO

Handling Editor: Professor Matthew Wright

*Keywords:*
Synthetic cathinones
Bioavailability
Apparent permeability (papp)
Cytotoxicity
Caco-2 cells
HepG2 cells

ABSTRACT

Understanding the biochemical effects of synthetic cathinone is essential to elucidate its pharmacological actions and systemic impact. Synthetic cathinones are β-keto amphetamine derivatives structurally related to cathinone, widely used as psychoactive substances and commonly consumed orally. In this study, the gastrointestinal permeation and hepatocellular responses of twelve chloro-cathinones were evaluated using complementary *in vitro* models. Differentiated Caco-2 monolayers demonstrated variable permeability, with 3-CIC (3-chloro-*N*-isopropylcathinone) and 4-CEC (4-chloro-*N*-ethylcathinone) exhibiting the highest apparent permeability (P*app* $7.75 \times 10^{-6}$ and $4.89 \times 10^{-6}$ *cm/s*). The cytotoxic profiles were evaluated in Caco-2 and HepG2 cells, $IC_{50}$ values ranged from 1.87 to 6.20 mM and from 0.80 to 3.10 mM, respectively. Among the tested compounds, 3-CEC (3-chloro-*N*-ethylcathinone) and 4-CEC exhibited the greatest potency. Cell-based assays demonstrated that 3-CIC and 4-CIC (4-chloro-*N*-isopropylcathinone) increased reactive oxygen species levels, suggesting a contribution of-oxidative stress-mediated damage to the cytotoxic effects of these cathinones. These findings provide new insights into the absorption properties of synthetic cathinones and their impact on liver cells, supporting the assessment of their health risks.

## 1. Introduction

Synthetic cathinones are β-keto amphetamine derivatives structurally related to cathinone, the psychoactive alkaloid of *Catha edulis*. They are consumed through several routes, including oral, nasal, intravenous, and rectal administration (Poyatos et al., 2021; Chen et al., 2024). Oral ingestion is the most common route typically producing slower, but more prolonged effects (Chen et al., 2024). Oral doses vary widely across compounds – for example, 15–250 mg for mephedrone (4-methylmethcathinone) (Dargan et al., 2011), 100–200 mg for methylone (Poyatos et al., 2021), 8–15 mg for MDPV (methylenedioxypyrovalerone) (EUDA, 2013), and 20–25 mg for α-PVP (α-pyrrolidinopentiophenone) (EUDA, 2016).

Drug bioavailability refers to the fraction of a dose that reaches systemic circulation. Knowledge of cathinones' bioavailability is essential for assessing their psychoactive and toxicological effects, predicting potential health risks, and guiding regulatory decisions regarding their classification, control, and public health management (Valente et al., 2014). The bioavailability of cathinones is largely determined by their ability to cross biological membranes, particularly the intestinal barrier. Structural characteristics are known to significantly affect membrane permeability, with certain cathinones exhibiting high permeability (Almeida et al., 2022). For example, 3,4-methylenedioxypyrovalerone (MDPV), a potent synthetic cathinone, exhibits high permeability through monolayers of Caco-2 cell – an established *in vitro* model of the human intestinal epithelium – suggesting high oral bioavailability (Almeida et al., 2023). Variability in the permeability of compounds such as methylone and pentedrone has also been reported, with some structural variants reaching apparent permeability coefficient (*Papp*) values in the moderate permeability range, with values of 5.28 ×

* Corresponding author. Centro de Química Estrutural, Institute of Molecular Sciences, Faculdade de Ciências, Universidade de Lisboa, 1749-016, Lisboa, Portugal.
** Corresponding author. Departamento de Química e Bioquímica, Faculdade de Ciências, Universidade de Lisboa, 1749-016, Lisboa, Portugal.
*E-mail addresses:* rita.pacheco@isel.pt (R. Pacheco), hmgaspar@ciencias.ulisboa.pt (H. Gaspar).
[1] These authors have contributed equally to this work and share senior authorship.

https://doi.org/10.1016/j.fct.2026.115981
Received 17 October 2025; Received in revised form 22 December 2025; Accepted 25 January 2026
Available online 26 January 2026

$10^{-6}$ *cm/s* and $5.18 \times 10^{-6}$ *cm/s*, respectively (Silva et al., 2020). *Papp* is a fundamental parameter used to quantify the rate at which a compound permeates across a biological barrier, typically in *in vitro* models such as Caco-2 cell monolayers that simulate the intestinal epithelium. These findings illustrate the sensitivity of permeability to subtle structural modifications. However, the relationship between structural diversity and intestinal permeability remains understood, particularly given the rapid emergence of new psychoactive cathinones.

In addition to bioavailability, assessing toxicity mechanisms of cathinones is important for understanding their potential health risks. Chronic or high-dose consumption of cathinones has been associated to a wide range of toxic effects, including hyperthermia, cardiovascular complications, organ failure, and death (Abebe et al., 2015; Silva et al., 2022). These toxic effects are often associated with mechanisms such as oxidative stress, mitochondrial dysfunction, and neurotoxicity, which can be exacerbated by the high bioavailability of these compounds in the bloodstream (Dargan et al., 2011; Gomes et al., 2025; Zwartsen et al., 2020).

Given the severity of their adverse effects, and the lack of studies evaluating how chloro-substitution or *N*-alkyl chain variations influence gastrointestinal permeability and hepatotoxicity, it is crucial to advance the understanding of these relationships. The present study aims to investigate both the bioavailability and the toxicity mechanisms of cathinones. Specifically evaluating the gastrointestinal bioavailability of twelve chloro-cathinones, using a Caco-2 model of the human intestinal barrier, to determine their potential to reach systemic circulation and potentially contribute to liver toxicity. Toxicity mechanisms were explored in HepG2 cells, a liver model cell line, reflecting the liver's key role in metabolizing and detoxifying harmful substances. This work provides the first systematic assessment of how chloro-substitution at *meta* and *para* positions modulates intestinal permeability and hepatic toxic effects, offering new insights into the structure–activity relationships of halogenated cathinones—a poorly characterized but increasingly prevalent subgroup in drug markets.

This study focused on seven cathinones (Fig. 1) already reported to the European Union Drugs Agency (EUDA); the illicit drugs 3-CMC (3-chloro-*N*-methylcathinone also known as clephedrone) and 4-CMC (4-chloro-*N*-methylcathinone); 3-Cl-TBC (3-chloro-*terc*-butylcathinone, commonly known as bupropion, an antidepressant medication used as a smoking cessation aid) (Huecker et al., 2024); as well as 3-CEC (3-chloro-*N*-ethylcathinone), 4-CEC (4-chloro-*N*-ethylcathinone), 4-CBC (4-chloro-*N*-butylcathinone), and 4-CIC (4-chloro-*N*-isopropylcathinone). Notably, in 2022, 3-CMC accounted for 73.26 % of all seized synthetic cathinones, totalling 26.5 tonnes (EUDA, 2025). Additionally, a set of five cathinones not yet reported in recreational drug markets was also investigated: 3-CBC (3-chloro-*N*-butylcathinone), 3-Cl-DEC (3-chloro-*N*,*N*-diethylcathinone), 4-Cl-DEC (4-chloro-*N*,*N*-diethylcathinone), 3-CIC (3-chloro-*N*-isopropylcathinone), 4-Cl-TBC (4-chloro-*terc*-butylcathinone) (Gomes et al., 2025). By assessing their absorption and cytotoxicity in human cell lines such as Caco-2 (intestinal model) and HepG2 (liver model), this study will contribute to a deeper understanding of how these compounds interact with the body and the underlying biological processes that lead to toxicity.

Understanding the bioavailability and toxicity mechanisms of cathinones is essential for predicting their health risks, establishing more effective harm reduction strategies, and providing regulatory bodies with critical information to address the emerging threat posed by these substances.

## 2. Materials and methods

### 2.1. Chemicals and biochemicals

*Roswell Park Memorial Institute* (RPMI) culture medium, *ultrapure dimethyl sulfoxide* (DMSO), *3-[4,5-dimethylthiazol*-2-yl*]-2,5-diphenyltetrazolium bromide* (MTT), *Dulbecco's Modified Eagle Medium* (DMEM) and inactivated *Fetal Bovine Serum* (FBS) from Biowest, *L-glutamine* 100x and *Trypsin* 10x from Lonza, *penicillin-streptomycin* solution 50x (Pen-strep) and *Phosphate-Buffered Saline* 1x (PBS) from Corning, *copper sulfate* (>99 %), *2′,7′-dichlorodihydrofluorescein diacetate* ($H_2$DCFDA), and *tert-butyl hydroperoxide* (TBHP) from Sigma, 96 % ethanol from Labchem, ultrapure water from Merck, *methanol* and *acetonitrile* from Honeywell, CyQUANT Lactate dehydrogenase (LDH, EC 1.1.1.27) Cytotoxicity Assay Kit (ThermoFisher Scientific). The *Hank's Balanced Salt Solution* (HBSS) was prepared using *D-glucose* from HiMedia, *anhydrous disodium phosphate* from Pancreac, *calcium chloride*, *sodium bicarbonate*, *monopotassium phosphate*, and *anhydrous magnesium sulfate* from Merck, *magnesium chloride hexahydrate* from Riedel-deHaen, *sodium chloride*, and *potassium chloride* from Fluka.The hydrochloride salt standards of the chlorinated cathinones used in this study were previously synthesized

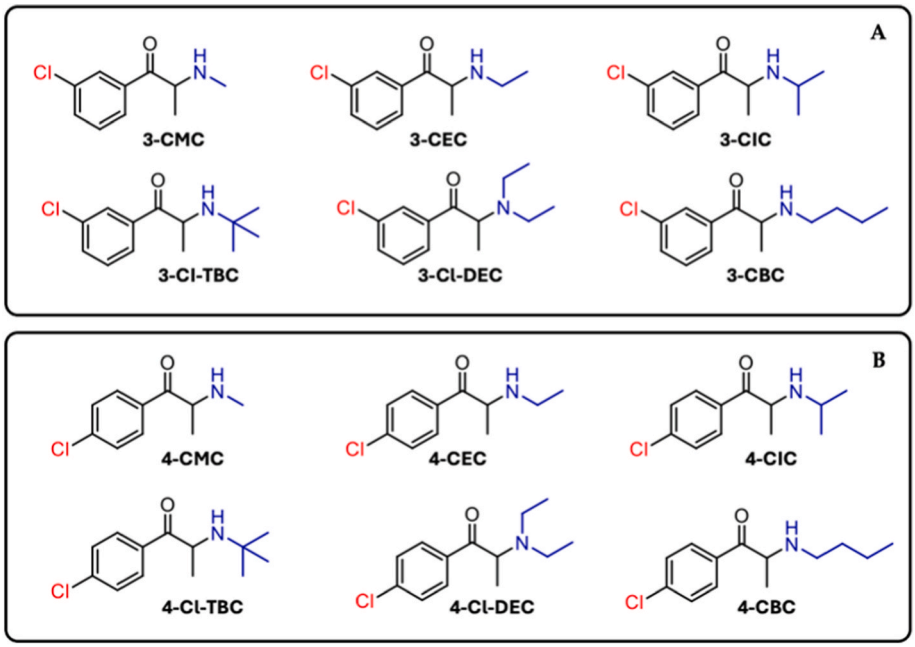


**Fig. 1.** Chemical structure of the studied cathinones, categorized by (A) *meta* and (B) *para* positions.

and characterized (Gomes et al., 2025).

### 2.2. Assessment of cytotoxicity by the MTT method

Caco-2 and HepG2 cells were cultured in t-flasks in a laminar flow chamber (ESCO Class II biohazard safety cabinet) using RPMI and DMEM media, respectively, supplemented with 10 % FBS, 1 % L-glutamine, and 1 % pen-strep, and placed in an incubator (Shen Lab) at 37 °C, 5 % $CO_2$, in a humid environment. After 2–3 days of culture in 96-well plates ($5.0 \times 10^4$ *cells/mL* for Caco-2 cells and $7.5 \times 10^4$ *cells/mL* for HepG2 cells) with 100 µL of media per well, the media was replaced with 100 µL of synthetic cathinones solutions (1–10 mM for Caco-2 cells and 0.3–6 mM for HepG2 cells) in FBS-free media, with ultrapure water as the control. The concentrations were selected based on preliminary cell viability results for each cell line (Gomes et al., 2025). This assay was performed at least once with six replicates (n = 3). After 24 h exposure, MTT assay was performed, and the absorbance was measured on a microplate reader (Tecan Sunrise) at 595 nm with a 630 nm reference to assess cell viability. Cytotoxicity was calculated using Equation (1), where CD represents cell death, $Abs_{control}$ is the absorbance of the control, and $Abs_{sample}$ is the absorbance with cathinone. The $IC_{50}$ values, representing the concentration of cathinone causing 50 % cell death, were determined using a non-linear regression model in *GraphPad Prism 10*.

$$CD\ (\%) = 100 - \left(\frac{Abs_{sample}}{Abs_{control}} \times 100\right) \quad (1)$$

### 2.3. Detection and quantification of cathinones by HPLC-DAD

For the quantification of cathinones, high-performance liquid chromatography coupled with diode array detection (HPLC-DAD) equipment (VWR Hitachi) with a reversed-phase ACE 3 C18 column (150 × 4.6 mm (ACE-111-1546) ACE) was used. The mobile phase consisted of acetonitrile (ACN) with 0.1 % formic acid and water with 0.1 % formic acid, in a gradient: 0–5 min (25 % ACN); 5–7 min (30 % ACN); 7–8 min (45 % ACN); 8–12 min (60 % ACN); 12–16 min (60 % ACN); 16–17 min (25 % ACN), at a flow rate of 1 mL/min and injection volume of 10 µL. The analysis was carried out with combined solutions (solution with all cathinones in the *meta* position and solution with all cathinones in the *para* position) at concentrations 1, 5, 10, 15, 20 and 25 µg/mL, injected in duplicate, on three different days.

### 2.4. Assessment of the permeability of the gastrointestinal barrier

Since gastrointestinal barrier permeability assays require differentiated Caco-2 cells that, after 21 days, form a monolayer mimicking the intestinal epithelium (Sambuy et al., 2005), Caco-2 cells were cultured at $3.4 \times 10^4$ *cells/well* in RPMI medium on polycarbonate Transwell inserts (A = 0.90 $cm^2$) in 12-well plates until full differentiation. The integrity of the cellular monolayer was confirmed by transepithelial electrical resistance (TEER), requiring values of ≥250 Ω/$cm^2$.

After differentiation, 0.5 mL of HBSS with synthetic cathinones at their $IC_{50}$ concentrations (determined by MTT assay) was added to the apical side, while 1 mL of HBSS was applied in the basolateral side. Caffeine and mannitol served as high and low permeability controls, respectively. Samples were collected at 0 h, 3 h, and 6 h, then frozen for HPLC-DAD analysis. The percentage of permeation was calculated assuming that the initial amount applied to the apical side corresponds to 100 %. The permeation of the samples was calculated using Equation (2), where C is the concentration.

$$Permeation\ (\%) = \left(\frac{C_{basolateral}}{C_{apical}} \times 100\right) \quad (2)$$

The apparent permeability coefficient (*Papp*) was calculated using Equation (3) to quantify the compounds, where V represents the volume of the receptor (basolateral side) in *mL*, A corresponds to the insert area in $cm^2$, and Δt represents the time variation in seconds. The concentrations (C) of the receptor and donor (apical side) are expressed in *mM*.

$$P_{app}\ (cm/s) = \frac{V_{basolateral} \times \Delta C_{basolateral}}{\Delta t \times A \times C_{apical\ t=0}} \quad (3)$$

### 2.5. Effects on the cell membrane by the lactate dehydrogenase (LDH) method

HepG2 cells were cultured in a 96-well microplate ($7.5 \times 10^4$ *cells/mL*) in triplicate wells (n = 3) with 100 µL of DMEM medium and incubated for 24 h. For LDH activity assessment, 10 µL of ultrapure water (Spontaneous LDH Activity) and cathinones at $IC_{50}$ concentrations determined by MTT assay were added and incubated for another 24h. A separate set of triplicates received 10 µL of Lysis Buffer (Maximum LDH Activity) and were incubated for 45 min. Afterward, 50 µL of each sample medium and 50 µL of Positive Control were transferred to a new plate, followed by 50 µL of Reaction Mixture. The negative control was performed in the absence of cathinone. The plate was incubated for 30 min, then 50 µL of STOP Solution was added. Absorbance was measured at 490 nm and 680 nm. This method detects LDH release as an indicator of cell membrane damage, indicating necrotic or apoptotic cell death caused by cathinones exposure (Forest et al., 2015; Kaja et al., 2017). The percentage of cytotoxicity was calculated from Equation (4).

$$Cytotoxicity\ (\%) = \left(\frac{Abs_{sample} - Abs_{Spontaneous\ Activity}}{Abs_{Maximum\ Activity} - Abs_{Spontaneous\ Activity}}\right) \times 100 \quad (4)$$

### 2.6. Reactive oxygen species (ROS) production

HepG2 cells were cultured in 96-well microplates ($2.5 \times 10^4$ *cells/mL*) with black walls and transparent bottoms, in triplicate wells (n = 3), using 100 µL of DMEM per well, and incubated for 24h. After washing the cells with PBS, 0.2 mM $H_2$-DCFDA solution was applied and incubated for 45 min, protected from light. The solution was removed, and 200 µM TBHP (positive control) was added, followed by 6 h incubation in the dark. Absorbance was measured using a fluorescence microplate reader with excitation at 495 nm, emission at 527 nm, medium sensitivity, and at 37 °C. This assay quantifies cathinone-induced reactive oxygen species (ROS) production by detecting the oxidation of $H_2$DCF to *2′,7′-dichlorofluorescein* (DCF) (Ng and Ooi, 2021). Oxidative stress was calculated from Equation (5).

$$Oxidative\ Stress\ (\%) = \left(\frac{Abs_{sample}}{Abs_{control}}\right) \times 100 \quad (5)$$

### 2.7. Statistical analysis

The statistical analysis was performed using Microsoft Office Excel, and results are expressed as mean ± standard deviation. Cytotoxicity data were assumed to be normally distributed based on the symmetry of the observed responses and the number of replicates per group. One-way analysis of variance (ANOVA) was used to assess differences among groups, followed by a Tukey's post hoc test to identify significant differences in $IC_{50}$ obtained from the MTT assay. Similarly, one-way ANOVA followed by a Tukey's post hoc test was applied to analyze the LDH assay and ROS production, differences were considered statistically significant at *p*-values below 0.05 ($p < 0.05$).

## 3. Results

### 3.1. Cytotoxicity of synthetic cathinones in undiferentiated Caco-2 and HepG2 cell lines

The cytotoxic effects of the selected chloro-cathinones were assessed in Caco-2 and HepG2 cells using the MTT assay, after 24 h exposure to

different concentration of cathinones, 1–10 mM for Caco-2 cells and 0.3–6 mM for HepG2 cells. Dose–response curves were constructed for each cathinone across both cell lines HepG2 (Fig. 2) and Caco-2 (Fig. 3) to assess their concentration-dependent cytotoxic effects. The figures group *meta* and *para* isomers together in the same plot to allow direct comparison of the cytotoxicity profiles.

From the nonlinear regression adjustment of the dose–response curves, the $IC_{50}$ values – defined as the cathinone concentration causing a 50 % reduction in cell viability – were obtained. Table 1 presents these $IC_{50}$ values along with their 95 % confidence intervals, the Hill slope parameter (indicating the steepest slope of the fitted curve), and the lowest observed adverse effect level (LOAEL) for each compound.

All tested cathinones exhibited cytotoxic and concentration-dependent cytotoxic effects on both cell lines, nevertheless it was seen that HepG2 demonstrated greater sensitivity compared to Caco-2 cells, with $IC_{50}$ values between 0.8 and 3.1 mM and 1.87–6.20, respectively In both cellular models it was noteworthy that the most cytotoxic cathinones were 3-CBC and its isomer 4-CBC, with both $IC_{50}$ values of 1.9 mM for Caco-2 cells, and 1.2 mM and 0.8 mM, respectively, for HepG2 cells.

However, 4-Cl-DEC, 3-Cl-DEC, and 3-CIC in Caco-2 cells, as well as 4-CIC and 3-Cl-DEC in HepG2 cells, exhibited relatively high Hill slope values (97.9, 35.8, and 28.9 for Caco-2; 35.6 and 35.0 for HepG2, respectively).

As Caco-2 cells must be fully differentiated to form a monolayer that mimics the intestinal epithelium for reliable gastrointestinal permeability assays, an additional MTT viability assessment was performed following the 21-day differentiation period. Differentiated Caco-2 cells were exposed to all 12 cathinones for 24 h, maintaining viability above 90 %. These results confirm the integrity and suitability of the differentiated monolayer for subsequent permeability testing.

### 3.2. Detection and quantification of cathinones by HPLC-DAD

Prior to conducting the permeability assays, HPLC-DAD analyses were performed to quantify and confirm the concentration of the twelve chloro-cathinones used in the experiments. This step ensured accurate dosing and reliable interpretation of the subsequent assay of the assessment of the permeability of the gastrointestinal barrier model.

An HPLC-DAD method was developed to detect and quantify the target cathinones (Fig. 1). Calibration standards were prepared at concentrations of 1, 5, 10, 15, 20, and 25 μg/mL in Hank's Balanced Salt Solution (HBSS) to match the conditions used in the permeability assays. These standards were injected in duplicate over three separate days to determine retention times and UV–Vis spectra, and to construct calibration curves. Table 2 presents the results of this analysis, including the errors in concentration determination, the limits of detection (LOD) and quantification (LOQ). Based on the obtained parameters, the suitability of the method for the detection and quantification of cathinones in the gastrointestinal barrier permeability assays was confirmed. Using this method, the permeability of the twelve chloro-cathinones was evaluated in differentiated Caco-2 cell monolayers.

### 3.3. Assessment of the permeability of the gastrointestinal barrier in differentiated Caco-2

For the gastrointestinal barrier permeability assay, differentiated Caco-2 monolayers were used after 21 days of culture. Transepithelial electrical resistance (TEER) measurements were performed to confirm monolayer integrity. Cathinone solutions prepared in HBSS were then applied to the apical side at their previously determined $IC_{50}$ concentrations by MTT assay. Permeation into the basolateral compartment was assessed after 3 and 6 h (Fig. 4). Based on Fig. 4, it was observed that after 6 h of incubation, 3-CIC and 4-CEC revealed the highest permeation rates with values of 15.07 % and 9.51 %, respectively. These results indicate that both compounds have a greater ability to permeate the gastrointestinal barrier. To further characterize the permeability of the tested cathinones, the apparent permeability coefficient (*Papp*) was calculated. Additionally, control assays using caffeine and mannitol were performed at a concentration of 0.8 mg/mL to support the method's effectiveness. The results of these calculations are presented in Table 3.

Based on the *Papp* values presented in Table 3, cathinones 3-CIC, 4-CEC, 4-CMC, 3-Cl-DEC, 3-CBC, 3-CEC, 3-CMC, 4-CBC, and 4-Cl-DEC exhibit moderate permeability, as their values fall within the range of $1.0–10 \times 10^{-6}$ cm/s. Among these, 3-CIC showed the highest *Papp* value of $7.75 \times 10^{-6}$ cm/s. In contrast, 4-CIC, 3-Cl-TBC, and 4-Cl-TBC, demonstrated low permeability, with *Papp* values below $1.0 \times 10^{-6}$

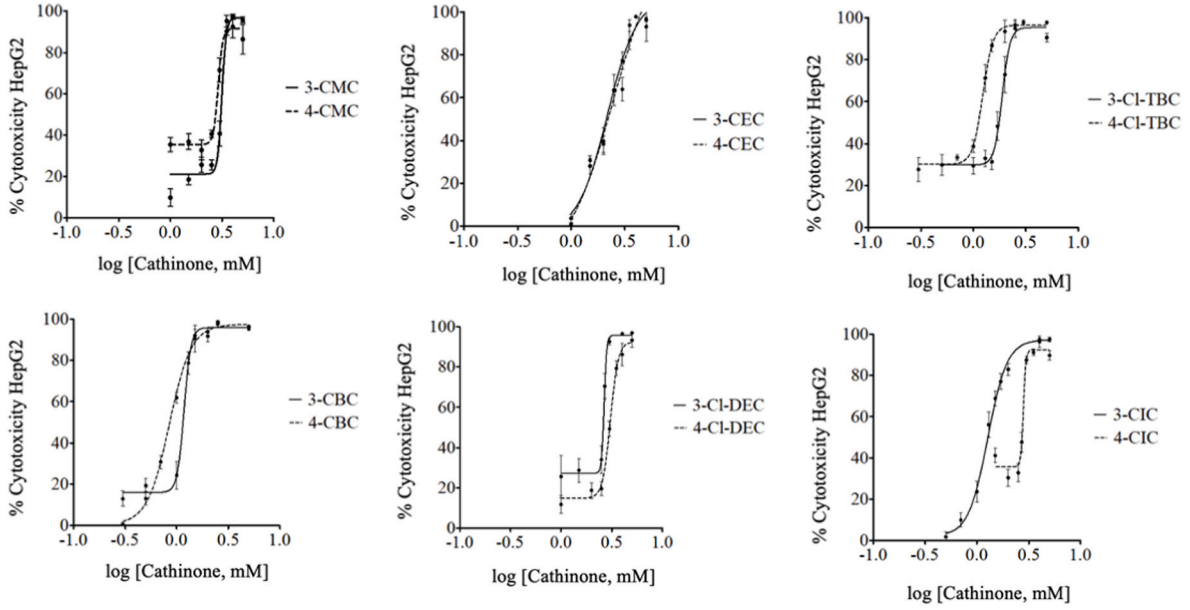


**Fig. 2.** Dose-response curves showing the percentage of cytotoxicity of the studied cathinones (0.3–6 mM), grouped by *meta*- and *para*-isomeric sets, as determined by the MTT reduction assay in HepG2 cells after 24 h of exposure. Cells incubated only in growth medium served as the control. Cytotoxicity values are expressed as mean ± standard deviation for each assay (n = 3, six technical replicates per assay).

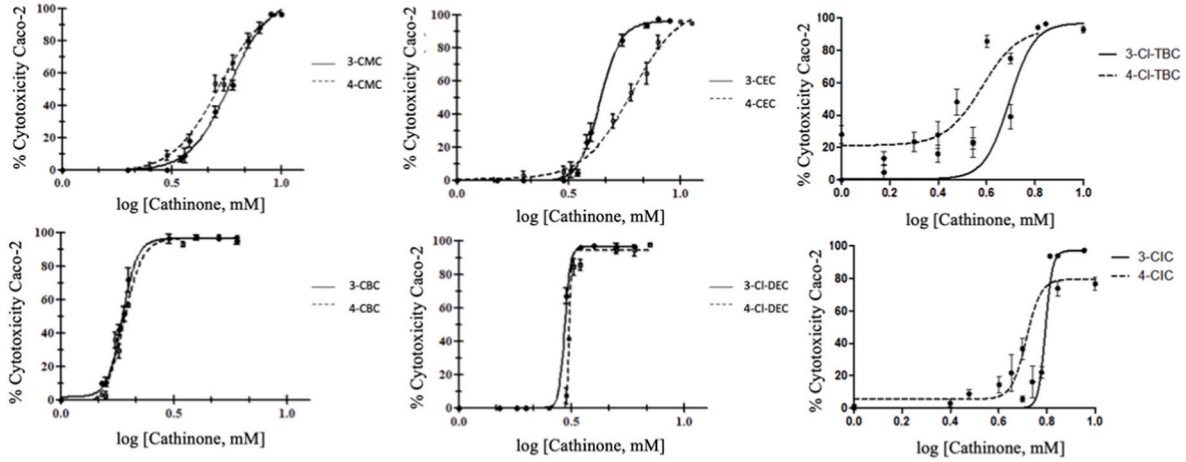


**Fig. 3.** Dose-response curves showing the percentage of cytotoxicity of the studied cathinones (1–10 mM), grouped by *meta*- and *para*-isomeric sets, as determined by the MTT reduction assay in Caco-2 cells after 24 h of exposure. Cells incubated only in growth medium served as the control. Cytotoxicity values are expressed as mean ± standard deviation (n = 3, six technical replicates per assay).

**Table 1**
Parameters derived from dose-response curves analysis of chloro-cathinones on Caco-2 (1–10 mM) and HepG2 (0.3–6 mM) cell lines, assessed using the MTT assay, $IC_{50}$ values (concentration causing 50 % reduction in cell viability), $p < 0.05$ confidence level, Hill slope coefficients (indicating curve steepness), and lowest observed adverse effect levels (LOAEL).

| Cathinone | $IC_{50}$ [CL] (mM) | | Hill Slope | | LOAEL (mM) | |
|---|---|---|---|---|---|---|
| | Caco-2 | HepG2 | Caco-2 | HepG2 | Caco-2 | HepG2 |
| **3-CMC** | 5.81 [5.38–6.28][a] | 3.10 [3.10–3.20][a] | 4.7 | 21.2 | 3.5 | 2.5 |
| **4-CMC** | 5.18 [4.68–5.72][b] | 2.90 [2.80–3.00][b] | 4.1 | 19.5 | 3.0 | 2.5 |
| **3-CEC** | 4.36 [4.22–4.50][c] | 2.20 [2.20–2.40][c] | 9.3 | 3.1 | 3.3 | 1.5 |
| **4-CEC** | 6.06 [5.48–6.65][ab] | 2.40 [1.90–3.20][d] | 4.1 | 2.1 | 3.5 | 1.5 |
| **3-CBC** | 1.87 [1.82–1.90][d] | 1.18 [1.16–1.20][e] | 13.4 | 13.1 | 1.3 | 1.0 |
| **4-CBC** | 1.90 [1.82–1.98][d] | 0.80 [0.80–0.90][f] | 10.8 | 4.1 | 1.5 | 0.5 |
| **3-Cl-DEC** | 2.95 [2.95–2.95][e] | 2.7 [2.60–2.70][g] | 35.8 | 35.0 | 2.3 | 2.5 |
| **4-Cl-DEC** | 3.098 [3.098–3.099][f] | 3.10 [3.00–3.10][a] | 97.9 | 11.3 | 3.0 | 2.5 |
| **3-CIC** | 6.20 [6.20–6.26][ab] | 1.30 [1.20–1.30][h] | 28.9 | 4.7 | 0.8 | 0.7 |
| **4-CIC** | 4.60 [4.44–4.71][c] | 2.80 [2.76–2.84][i] | 13.5 | 35.6 | 0.6 | 2.5 |
| **3-Cl-TBC** | 4.30 [4.20–4.43][c] | 1.90 [1.80–1.90][j] | 9.6 | 11.6 | 0.5 | 1.5 |
| **4-Cl-TBC** | 2.50 [2.39–2.75][g] | 1.20 [1.20–1.30][k] | 6.5 | 8.9 | 0.2 | 1.0 |

(a–k) Different letters indicate statistically significant differences among $IC_{50}$ values at $p < 0.05$, according to one-way ANOVA followed by an unpaired *t*-test for multiple comparisons.

**Table 2**
Retention times, detection wavelengths, and calibration curves parameters for the developed HPLC-DAD method used for identification and quantification of cathinones. For each cathinone, the calibration curve parameters include slope, y-intercept, coefficient of determination ($R^2$), concentration determination error (Error), limit of detection (LOD), and limit of quantification limit (LOQ), in μg/mL.

| Cathinone | Retention time (min) | λ (nm) | Slope | y-intercept | $R^2$ | Error | LOD (μg/mL) | LOQ (μg/mL) |
|---|---|---|---|---|---|---|---|---|
| **3-CMC** | 5.60 | 255 | 278931 | 84975 | 0.9995 | 0.2 | $2.8 \times 10^{-6}$ | $8.4 \times 10^{-6}$ |
| **4-CMC** | 5.90 | 265 | 248083 | 55544 | 0.9993 | 0.3 | $3.6 \times 10^{-6}$ | $1.1 \times 10^{-5}$ |
| **3-CEC** | 6.60 | 255 | 269995 | 77160 | 0.9996 | 0.2 | $2.6 \times 10^{-6}$ | $7.9 \times 10^{-6}$ |
| **4-CEC** | 6.80 | 265 | 195972 | 35731 | 0.9995 | 0.2 | $4.0 \times 10^{-6}$ | $1.2 \times 10^{-5}$ |
| **3-CBC** | 13.80 | 255 | 208532 | −1169.6 | 0.9992 | 0.3 | $4.4 \times 10^{-6}$ | $1.3 \times 10^{-5}$ |
| **4-CBC** | 13.60 | 265 | 359532 | 81360 | 0.9998 | 0.2 | $1.4 \times 10^{-6}$ | $4.3 \times 10^{-6}$ |
| **3-Cl-DEC** | 8.40 | 255 | 132151 | 198107 | 0.9976 | 0.5 | $1.2 \times 10^{-6}$ | $3.7 \times 10^{-5}$ |
| **4-Cl-DEC** | 8.60 | 265 | 346724 | 54868 | 0.9994 | 0.3 | $2.4 \times 10^{-6}$ | $7.3 \times 10^{-6}$ |
| **3-CIC** | 4.20 | 255 | 130868 | 26926 | 0.9995 | 0.3 | $8.3 \times 10^{-6}$ | $2.5 \times 10^{-5}$ |
| **4-CIC** | 4.50 | 265 | 74744 | 1854.3 | 0.9990 | 0.4 | $1.1 \times 10^{-5}$ | $3.4 \times 10^{-5}$ |
| **3-Cl-TBC** | 5.80 | 255 | 167284 | 10714 | 0.9984 | 0.5 | $1.5 \times 10^{-5}$ | $4.5 \times 10^{-5}$ |
| **4-Cl-TBC** | 6.20 | 265 | 258691 | −142234 | 0.9967 | 0.6 | $1.7 \times 10^{-5}$ | $5.2 \times 10^{-5}$ |

cm/s. The control compounds, mannitol and caffeine, displaying low and high permeability, respectively.

### *3.4. Assessment of toxicity mechanisms: effects on the cell membrane and ROS induction in HepG2*

The cathinone 3-CIC exhibited the highest gastrointestinal barrier permeability ($7.75 \times 10^{-6}$ *cm/s*) therefore it was selected for further investigation along with its isomer, 4-CIC, which showed low

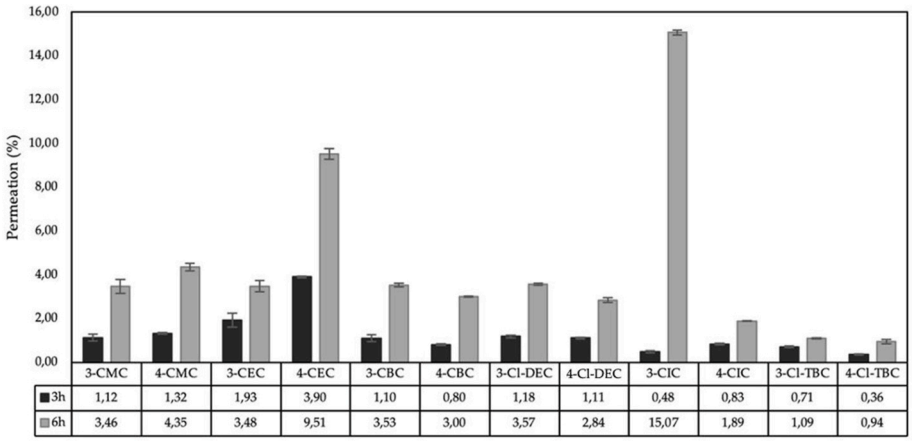


**Fig. 4.** Permeation (%) of the cathinones under study at the basolateral side, after 3 and 6 h of incubation, at $IC_{50}$ concentrations determined by MTT assay in Caco-2 cells. Caffeine and mannitol served as high and low permeability controls, respectively (n = 3, with three replicates).

**Table 3**
Results of the apparent permeability coefficient (*Papp*) of the tested cathinones after 6 h of incubation. Caffeine and mannitol were assayed representing reference compounds with high and low permeability controls, respectively.

| Cathinone | *Papp* (x$10^{-6}$ cm/s) |
|---|---|
| **3-CMC** | 1.78 |
| **4-CMC** | 2.24 |
| **3-CEC** | 1.79 |
| **4-CEC** | 4.89 |
| **3-CBC** | 1.82 |
| **4-CBC** | 1.54 |
| **3-Cl-DEC** | 1.84 |
| **4-Cl-DEC** | 1.46 |
| **3-CIC** | 7.75 |
| **4-CIC** | 0.97 |
| **3-Cl-TBC** | 0.56 |
| **4-Cl-TBC** | 0.48 |
| **Mannitol** | 0.08 |
| **Caffeine** | 15.00 |

permeability. These two compounds, representing the highest and lowest P*app* values in the isopropyl series, provide a contrasting pair ideal for assessing how the position of the chlorine atom influences hepatic toxicity. These analyses focused on effects related to cell membrane integrity and ROS induction in liver HepG2 cells.

To evaluate the effect of these cathinones on cell membrane integrity, the LDH assay was performed. Additionally, the $H_2$DCFDA assay was conducted to evaluate cathinone-induced ROS production. The results of both assays are presented in Figs. 5 and 6, respectively. The results indicate that both 3-CIC and 4-CIC exert moderate cytotoxic effects on HepG2 cells by compromising the membrane integrity, with slightly higher effects observed for 4-CIC, as reflected by LDH release values of 21.3 % and 27.1 %, respectively. Notably, both compounds induced increases in ROS levels, again with a more pronounced effect for 4-CIC (476.8 % relative to control) compared with 3-CIC (355.9 %). This significant elevation in reactive oxygen species suggests that oxidative damage may be a key mechanism underlying the cell death observed in liver cells due to exposure to these cathinones.

## 4. Discussion

This study presents the first report of the gastrointestinal permeability and hepatoxicity of the twelve chloro-cathinones presented in Fig. 1. The cathinones were selected based on: (i) their recent prevalence in EUDA alerts, (ii) structural diversity in both amino group and chlorine atom position on aromatic ring, and iii) the inclusion of five previously unreported analogues, in order to obtain a diverse set of cathinones to

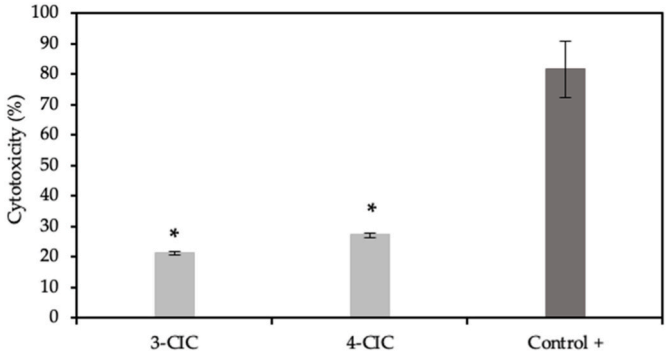


**Fig. 5.** Membrane damage-induced cytotoxicity by LDH assay in HepG2 cells exposed to 3-CIC and 4-CIC, after 24 h of incubation, at their $IC_{50}$ concentration determined by MTT assay. The positive control was included as provided by the assay kit and negative control was performed in the absence of cathinone (n = 3, with three replicates). (*) Indicates a statistically significant difference compared to the positive control with 3-CIC ($p$ = 0.0065) and 4-CIC ($p$ = 0.0003), according to one-way ANOVA.

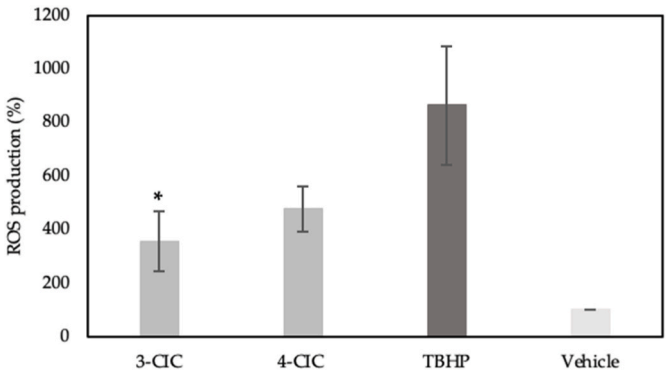


**Fig. 6.** Percentage of ROS production in HepG2 cells exposed to 3-CIC and 4-CIC, after 24 h of incubation, at $IC_{50}$ concentration determined by MTT assay. *Tert*-butyl hydroperoxide (TBHP) was used as positive control, and a non-treated group of cells exposed to the vehicle served as the negative control (n = 3, with three replicates). (*) Indicates statistically significant differences compared to the positive control (TBHP) with $p$ =*0.0228*, according to one-way ANOVA.

understand the influence of structural features on the observed effects.

In the gastrointestinal permeability studies, 3-CIC and 4-CEC, exhibited the highest permeation rates after 6 h of incubation, 15.1 % and 9.5 %, respectively. According to the classification criteria proposed by Angelis and Turco (2011), both cathinones showed moderate permeability, with apparent permeability coefficients (*Papp*) of $7.75 \times 10^{-6}$ *cm/s* and $4.89 \times 10^{-6}$ *cm/s*, respectively. In contrast, 4-Cl-TBC, 3-Cl-TBC, and 4-CIC displayed lower permeation rates of 0.9 %, 1.1 %, and 1.9 %, respectively, corresponding to low permeability as their *Papp* $< 1.0 \times 10^{-6}$ *cm/s*). The results obtained with the reference compounds, caffeine (*Papp* $= 15 \times 10^{-6}$ *cm/s*) and mannitol (*Papp* $= 0.08 \times 10^{-6}$ *cm/s*), validated the assay sensitivity and monolayer integrity, as these compounds are reported as high- and low-permeability standards, respectively (Usansky and Sinko, 2005).

Overall, the results obtained indicate that neither the chloro-substitution position nor the *N*-alkyl chain in the tested cathinones appears to significantly influence their permeability. Most cathinones showed P*app* values within the range of 0.48 and $2.24 \times 10^{-6}$ *cm/s*, with the *meta*- and its corresponding *para*-isomer for all analogues generally exhibiting similar permeability. The only exceptions were for the CEC and CIC isomers, which displayed 3-fold and 8-fold differences between isomers *Papp* values, respectively, suggesting that, for these cathinones, the position of the chlorine atom influences their permeability.

Although limited, studies have been conducted on the permeability of synthetic cathinones. Silva et al. (2020) investigated the enantiomeric permeability of methylone and pentedrone using Caco-2 cell monolayers. Their findings revealed no enantioselective permeability with pentedrone exhibiting similar *Papp* values of moderate permeability ($5.28 \times 10^{-6}$ *cm/s S*-isomer;- and $5.81 \times 10^{-6}$ *cm/s R*-isomer). For methylone, only slight differences were obtained in *Papp* values between enantiomers ($5.18 \times 10^{-6}$ *cm/s S*-isomer;- and $3.46 \times 10^{-6}$ *cm/s R*-isomer). Similarly, Almeida et al. (2023) focused on MDPV enantiomers, observing no enantioselective permeability in the apical to basolateral direction, with both exhibiting high permeability (*Papp* values $1.8 \times 10^{-5}$ *cm/s*) through the Caco-2 monolayer, indicating significant intestinal absorption potential.

Reported human plasma levels after recreational consumption of synthetic cathinones are typically in the *ng/mL* to *μM* range. Pharmacokinetic data showed that mephedrone exhibits plasma concentrations ranging from 1 to 1060 ng/mL after oral administration, MDPV between 1 and 8400 ng/mL, methylone from <1 to 4400 ng/mL, α-PVP between <1 and 606 ng/mL and 4-CEC around 2 ng/mL (Adamowicz, 2021). These variations reflect the structural and pharmacokinetic differences between the compounds, as well as individual biological factors and the method of administration. After oral ingestion of synthetic cathinones, the plasma concentrations vary significantly depending on factors such as the dose, individual metabolism, and the route of administration. Once cathinones enter systemic circulation, they are distributed to various tissues, where their accumulation and interaction with cellular targets may lead to cytotoxic effects. The cathinones concentrations required to induce cytotoxicity *in vitro* usually fall within the millimolar range serving to compare relative potencies and to provide insight into potential *in vivo* exposure effects.

Analysis of the permeability data obtained in this study, together with the cell-death results in HepG2 cells, revealed that 3-CIC, which showed the highest permeability, also exhibited high hepatic cytotoxicity, with an $IC_{50}$ value of 1.30 mM. This suggests that 3-CIC may pose a greater health risk to the liver and potentially to other internal organs. Interestingly, 3-CBC and 4-CBC, which showed the highest cytotoxicity in both HepG2 cells and Caco-2 cells, were also identified previous studies as the most cytotoxic in the SH-SY5Y cell line (Gomes et al., 2025; Lopes et al., 2025). This trend across different cell models suggests that the *N*-butyl substituent may be a key structural feature contributing to the cytotoxic effects of cathinones.

In addition, some cathinones exhibited remarkably steep dose–response curves, particularly 4-Cl-DEC, 3-Cl-DEC, and 3-CIC in Caco-2 cells, as well as 4-CIC and 3-Cl-DEC in HepG2 cells, which exhibited high Hill slope values (97.9, 35.8, and 28.9 for Caco-2 and 35.6 and 35.0 for HepG2, respectively). These steep slopes indicate that small variations in concentration can lead to pronounced increases in cytotoxicity, reflecting a more pronounced toxicity profile. This behavior suggests that, under certain exposure conditions, these compounds may pose a higher toxicological risk compared to other cathinones, even when $IC_{50}$ values are similar. This steep dose–response behavior may reflect differences in cellular uptake, membrane interaction, or intracellular accumulation thresholds of compounds (Smit et al., 2001).

Overall, it was also observed that the cathinones tested exhibited greater toxicity in HepG2 liver cells, indicating that these cells are more susceptible to cytotoxic effects than Caco-2 intestinal cells. Caco-2 cells, particularly when differentiated, simulate an epithelial barrier with high TEER values and tight junctions that limit the entry of toxic compound, as demonstrated by Darling et al. (2020) and also observed in this study. In contrast, HepG2 cells lack barrier properties and are more susceptible to toxicity due to limited transporter expression and reduced efflux capacity, as demonstrated by Hilgendorf et al. (2007) and Rodrigues et al. (2009). In addition, HepG2 cells are also characterized by high metabolic activity due to the expression of hepatic enzymes, including the cytochrome P450 system, which are involved in the metabolism of chemical compounds. Ma et al. (2016) reported that the high metabolic activity of HepG2 cells can lead to increased production of ROS, further contributing to cellular damage.

Regarding the mechanisms of cathinone-induced toxicity in the liver, the results showed that both 3-CIC and 4-CIC moderately affect HepG2 cell membrane integrity and induced high levels of ROS production, with slightly higher effects observed for 4-CIC. Comparison of the molecular structures of 4-CIC and 3-CIC (Fig. 1) reveals that the only difference between the two compounds is the position of the chlorine atom on the aromatic ring. This structural variation may be associated with the observed differences in ROS production and membrane damage, potentially reflecting a higher reactivity or affinity of 4-CIC for cellular targets including the membrane (Nadal-Gratacós et al., 2021; Zhao et al., 2017; Arias et al., 2012). However, these findings remain correlative and future targeted assays will clarify whether oxidative stress plays a role in the mechanism of toxicity of 3-CIC and 4-CIC, as well as support structural-activity relationship trends.

Luethi et al. (2017) demonstrated that other synthetic cathinones, including MDPV, induce concentration-dependent cell death in HepG2 cells, as evidenced by LDH release. These compounds significantly increase ROS production in HepG2 cells, suggesting that oxidative stress is also a key mechanism underlying their toxicity. Excess ROS can attack cellular membrane phospholipids, which can compromise membrane integrity, exacerbate cellular damage, and promote apoptosis or necrosis (Gaschler and Stockwell, 2017).

These findings underscore the importance in determining the toxicological profiles of synthetic cathinones, highlighting how specific structural features influence their biological effects. The correlation between permeability and cytotoxicity—particularly in cathinones like 3-CIC—suggests that intestinal absorption plays a critical role in systemic exposure and potential organ toxicity, especially in the liver.

Taken together, this study not only advances the understanding of gastrointestinal permeability of these twelve chloro-cathinones, but also provides mechanistic insight into their cytotoxic effects, particularly in the liver via oxidative stress. However, it is important to recognize that the experiments were conducted under *in vitro* conditions and employed cathinone concentrations that may not accurately reflect those found in physiological or real-world exposure scenarios. Given the limited data available on the actual concentrations present in users and considering that these compounds are drugs of abuse with increasing public health relevance, further investigation is essential. Continued research into their toxicodynamic behaviour, including studies using complementary *in vitro* and *in vivo* models, will be critical to better understand their effects and support more accurate risk assessments.

## 5. Conclusions

Based on the results obtained for the twelve synthetic cathinones tested and considering their oral route of consumption, 4-CEC and 3-CIC showed the highest bioavailability, as evidenced by greater permeability through the gastrointestinal barrier. These findings suggest that these cathinones may more easily reach the systemic circulation and potentially affect organs, particularly the liver with 3-CIC posing the greatest concern due to its higher toxicity in HepG2 cells. Furthermore, the data indicates that exposure to 3-CIC or its isomer, 4-CIC, induces ROS production and compromises cell membrane integrity which may reduce cell viability. Overall, the results of this study provide new insights into the structural and toxicological characteristics of synthetic cathinones, specifically highlighting the relationship between chemical structure and their cytotoxicity and permeability profiles.

## CRediT authorship contribution statement

**Mariana Meneses:** Writing – review & editing, Writing – original draft, Formal analysis. **Inês Ferreira:** Writing – review & editing, Formal analysis. **Ana Patrícia Gomes:** Writing – review & editing, Formal analysis. **Rita Pacheco:** Writing – review & editing, Supervision, Project administration, Methodology, Funding acquisition, Conceptualization. **Helena Gaspar:** Writing – review & editing, Supervision, Project administration, Methodology, Funding acquisition, Conceptualization.

## Declaration of generative AI and AI-assited technologies in the manuscript preparation process

During the preparation of this work, the author(s) used Chat GPT and DeepL Write in order improve the readability and language of the manuscript. After using this tool/service, the author(s) reviewed and edited the content as needed and take(s) full responsibility for the content of the published article.

## Funding sources

This research was financed by Centro de Química Estrutural funded by Portuguese Foundation for Science and Technology (FCT) through projects UIDB/00100/2020 and UIDP/00100/2020. Institute of Molecular Sciences is an Associate Laboratory funded by FCT through project LA/P/0056/2020. Work supported by UID/04046/2023 - Biosystems and Integrative Sciences Institute Centre grant from FCT, Portugal.

## Declaration of competing interest

The authors declare that they have no known competing financial interests or personal relationships that could have appeared to influence the work reported in this paper.

## Acknowledgments

This research was financed by Centro de Química Estrutural funded by Foundation for Science and Technology, FCT, Portugal through projects UID/00100/2025 and UID/PRR/100/2025. Institute of Molecular Sciences is an Associate Laboratory funded by FCT through project LA/P/0056/2020. Work supported by UID/04046/2025 - Biosystems and Integrative Sciences Institute Centre grant from FCT, Portugal.

## Glossary

| | |
|---|---|
| CAN | Acetonitrile |
| α-PVP | α-pyrrolidinopentiophenone |
| 3-CBC | 3-chloro-*N*-butylcathinone |
| 3-CEC | 3-chloro-*N*-ethylcathinone |
| 3-CIC | 3-chloro-*N*-isopropylcathinone |
| 3-Cl-DEC | 3-chloro-*N*,*N*-diethylcathinone |
| 3-Cl-TBC | 3-chloro-*terc*-butylcathinone |
| 3-CMC | 3-chloro-*N*-methylcathinone |
| 4-CBC | 4-chloro-*N*-butylcathinone |
| 4-CEC | 4-chloro-*N*-ethylcathinone |
| 4-CIC | 4-chloro-*N*-isopropylcathinone |
| 4-Cl-DEC | 4-chloro-*N*,*N*-diethylcathinone |
| 4-Cl-TBC | 4-chloro-*terc*-butylcathinone |
| 4-CMC | 4-chloro-*N*-methylcathinone |
| Caco-2 | Colorectal adenocarcinoma cell line |
| DCF | 2′,7′-dichlorofluorescein |
| DMEM | Dulbecco's Modified Eagle Medium |
| DMSO | Dimethyl sulfoxide |
| EUDA | European Union Drugs Agency |
| FBS | Fetal Bovine Serum |
| HBSS | Hank's Balanced Salt Solution |
| $H_2$DCF | 2′,7′-dichlorodihydrofluorescein |
| $H_2$DCFDA | 2′,7′-dichlorodihydrofluorescein diacetate |
| HepG2 | Hepatocellular carcinoma cell line |
| HPLC-DAD | High Performance Liquid Chromatography – Diode Array Detection |
| $IC_{50}$ | Concentration required to cause 50 % cell death |
| LDH | Lactate dehydrogenase |
| LOAEL | Lowest-observed-adverse-effect level |
| LOD | Limit of detection |
| LOQ | Limit of quantification |

## Data availability

Data will be made available on request.

## References


Abebe, M., Kindie, S., Adane, K., 2015. Adverse health effects of khat: a review. Fam. Med. Med. Sci. Res. 4 (1), 1000154. https://doi.org/10.4172/2327-4972.1000154.

Adamowicz, P., 2021. Blood concentrations of synthetic cathinones. Clin. Toxicol. 59 (7), 648–654. https://doi.org/10.1080/15563650.2020.1848100.

Almeida, A.S., Silva, B., de Pinho, P.G., Remião, F., Fernandes, C., 2022. Synthetic cathinones: recent developments, enantioselectivity studies and enantioseparation methods. Molecules 27 (7), 2057. https://doi.org/10.3390/molecules27072057.

Almeida, A.S., Silva, B., Remião, F., Fernandes, C., 2023. Assessment of the permeability of 3,4-Methylenedioxypyrovalerone (MDPV) across the Caco-2 monolayer for estimation of intestinal absorption and enantioselectivity. Int. J. Mol. Sci. 24 (3), 2680. https://doi.org/10.3390/ijms24032680.

Angelis, I.D., Turco, L., 2011. Caco-2 cells as a model for intestinal absorption. Curr. Protoc. Toxicol. 20. https://doi.org/10.1002/0471140856.tx2006s47. Unit20.6.

Arias, H.R., Feuerbach, D., Targowska-Duda, K.M., Aggarwal, S., Lapinsky, D.J., Jozwiak, K., 2012. Structural and functional interaction of (±)-2-(N-tert-butylamino)-3'-iodo-4'-azidopropiophenone, a photoreactive bupropion derivative, with nicotinic acetylcholine receptors. Neurochem. Int. 61 (8), 1433–1441. https://doi.org/10.1016/j.neuint.2012.10.011.

Chen, S., Zhou, W., Lai, M., 2024. Synthetic cathinones: epidemiology, toxicity, potential for abuse, and current public health perspective. Brain Sci. 14 (4), 334. https://doi.org/10.3390/brainsci14040334.

Dargan, P.I., Sedefov, R., Gallegos, A., Wood, D.M., 2011. The pharmacology and toxicology of the synthetic cathinone mephedrone (4-methylmethcathinone). Drug Test. Anal. 3 (7–8), 454–463. https://doi.org/10.1002/dta.312.

Darling, N.J., Mobbs, C.L., González-Hau, A.L., Freer, M., Przyborski, S., 2020. Bioengineering novel in vitro Co-culture models that represent the human intestinal mucosa with improved Caco-2 structure and barrier function. Front. Bioeng. Biotechnol. 8, 992. https://doi.org/10.3389/fbioe.2020.00992.

European Union Drugs Agency, 2013. MDPV: joint reports. https://www.euda.europa.eu/system/files/media/publications/documents/819/TDAS14001ENN_466653.pdf. (Accessed 25 November 2024).

European Union Drugs Agency, 2016. α-PVP: risk assessments. https://www.euda.europa.eu/system/files/publications/1814/TDAS15001ENN.pdf. (Accessed 27 November 2024).

European Union Drugs Agency, 2025. European drug report 2024: trends and developments. https://www.euda.europa.eu/publications/european-drug-report/2024_en. (Accessed 10 August 2024).

Forest, V., Figarol, A., Boudard, D., Cottier, M., Grosseau, P., Pourchez, J., 2015. Adsorption of lactate dehydrogenase enzyme on carbon nanotubes: how to get accurate results for the cytotoxicity of these nanomaterials. Langmuir 31 (12), 3635–3643. https://doi.org/10.1021/acs.langmuir.5b00631.

Gaschler, M.M., Stockwell, B.R., 2017. Lipid peroxidation in cell death. Biochem. Biophys. Res. Commun. 482 (3), 419–425. https://doi.org/10.1016/j.bbrc.2016.10.086.

Gomes, A.P., Ferro, R., Pinto, D., Silva, J., Alves, C., Pacheco, R., Gaspar, H., 2025. Synthesis, characterization, and biological effects of chloro-cathinones: toxicity and potential neurological impact. Int. J. Mol. Sci. 26 (8), 3540. https://doi.org/10.3390/ijms26083540.

Hilgendorf, C., Ahlin, G., Seithel, A., Artursson, P., Ungell, A.L., Karlsson, J., 2007. Expression of thirty-six drug transporter genes in human intestine, liver, kidney, and organotypic cell lines. Drug Metab. Dispos. 35 (8), 1333–1340. https://doi.org/10.1124/dmd.107.014902.

Huecker, M.R., Smiley, A., Saadabadi, A., 2024. Bupropion. In: StatPearls. Treasure Island (FL). StatPearls Publishing. https://www.ncbi.nlm.nih.gov/books/NBK470212/.

Kaja, S., Payne, A.J., Naumchuk, Y., Koulen, P., 2017. Quantification of lactate dehydrogenase for cell viability testing using cell lines and primary cultured astrocytes. Curr. Protoc. Toxicol. 2017, 1–10. https://doi.org/10.1002/cptx.21.

Lopes, R.P., Miranda, C.C., Fernandes, T.G., Gaspar, H., Antunes, A.M.M., 2025. The cytotoxicity of synthetic cathinones on dopaminergic-differentiated SH-SY5Y neuroblastoma cell line: exploring the role of β-keto metabolic reduction. Food Chem. Toxicol. 204, 115658. https://doi.org/10.1016/j.fct.2025.115658.

Luethi, D., Liechti, M.E., Krähenbühl, S., 2017. Mechanisms of hepatocellular toxicity associated with new psychoactive synthetic cathinones. Toxicol 387, 57–66. https://doi.org/10.1016/j.tox.2017.06.004.

Ma, Z., Li, C., Qiao, Y., Lu, C., Li, J., Song, W., Sun, J., Zhai, X., Niu, J., Ren, Q., Wen, A., 2016. Safflower yellow B suppresses HepG2 cell injury induced by oxidative stress through the AKT/Nrf2 pathway. Int. J. Mol. Med. 37 (3), 603–612. https://doi.org/10.3892/ijmm.2016.2462.

Nadal-Gratacós, N., Alberto-Silva, A.S., Rodríguez-Soler, M., Urquizu, E., Espinosa-Velasco, M., Jäntsch, K., Holy, M., Batllori, X., Berzosa, X., Pubill, D., Camarasa, J., Sitte, H.H., Escubedo, E., López-Arnau, R., 2021. Structure–activity relationship of novel second-generation synthetic cathinones: mechanism of action, locomotion, reward, and immediate-early genes. Front. Pharmacol. 12, 749429. https://doi.org/10.3389/fphar.2021.749429.

Ng, N.S., Ooi, L., 2021. A simple microplate assay for reactive oxygen species generation and rapid cellular protein normalization. Bio-Protocol. 11 (1), e3877. https://doi.org/10.21769/BioProtoc.3877.

Poyatos, L., Papaseit, E., Olesti, E., Pérez-Mañá, C., Ventura, M., Carbón, X., Grifell, M., Fonseca, F., Torrens, M., de la Torre, R., Farré, M., 2021. A comparison of acute pharmacological effects of methylone and mdma administration in humans and oral fluid concentrations as biomarkers of exposure. Biology 10 (8), 788. https://doi.org/10.3390/biology10080788.

Rodrigues, A.C., Curi, R., Dalla, F., Genvigir, V., Hirata, M.H., Dominguez, R., Hirata, C., 2009. The expression of efflux and uptake transporters are regulated by statins in Caco-2 and HepG2 cells. Acta Pharmacol. Sin. 30, 956–964. https://doi.org/10.1038/aps.2009.85.

Sambuy, Y., De Angelis, I., Ranaldi, G., Scarino, M.L., Stammati, A., Zucco, F., 2005. The Caco-2 cell line as a model of the intestinal barrier: influence of cell and culture-related factors on Caco-2 cell functional characteristics. Cell Biol. Toxicol. 21 (1), 1–26. https://doi.org/10.1007/s10565-005-0085-6.

Silva, B., Silva, R., Fernandes, C., Guedes de Pinho, P., Remião, F., 2020. Enantioselectivity on the absorption of methylone and pentedrone using Caco-2 cell line: development and validation of an UHPLC method for cathinones quantification. Toxicol. Appl. Pharmacol. 395, 114970. https://doi.org/10.1016/j.taap.2020.114970.

Silva, B., Soares, J., Rocha-Pereira, C., Mladěnka, P., Remião, F., On Behalf of The Oemonom Researchers, 2022. Khat, a cultural chewing drug: a toxicokinetic and toxicodynamic summary. Toxins 14 (2), 71. https://doi.org/10.3390/toxins14020071.

Smit, M.G., Hendriks, A.J., Schobben, J.H., Karman, C.C., Schobben, H.P., 2001. The variation in slope of concentration-effect relationships. Ecotoxicol. Environ. Saf. 48 (1), 43–50. https://doi.org/10.1006/eesa.2000.1983.

Usansky, H.H., Sinko, P.J., 2005. Estimating human drug oral absorption kinetics from Caco-2 permeability using an absorption-disposition model: model development and evaluation and derivation of analytical solutions for k(a) and f(a). J. Pharmacol. Exp. Ther. 314 (1), 391–399. https://doi.org/10.1124/jpet.104.076182.

Valente, M.J., Guedes de Pinho, P., de Lourdes Bastos, M., Carvalho, F., Carvalho, M., 2014. Khat and synthetic cathinones: a review. Arch. Toxicol. 88 (1), 15–45. https://doi.org/10.1007/s00204-013-1163-9.

Zhao, W., Feng, H., Sun, W., Liu, K., Lu, J.J., Chen, X., 2017. Tert-butyl hydroperoxide (t-BHP) induced apoptosis and necroptosis in endothelial cells: roles of NOX4 and mitochondrion. Redox Biol. 11, 524–534. https://doi.org/10.1016/j.redox.2016.12.036.

Zwartsen, A., Olijhoek, M.E., Westerink, R.H.S., Hondebrink, L., 2020. Hazard characterization of synthetic cathinones using viability, monoamine reuptake, and neuronal activity assays. Front. Neurosci. 14. https://doi.org/10.3389/fnins.2020.00009.